

Microscopy in 3D: a biologist's toolbox

Robert S. Fischer¹, Yicong Wu², Pakorn Kanchanawong³, Hari Shroff² and Clare M. Waterman¹

¹ National Heart Lung and Blood Institute, National Institutes of Health, Bethesda, MD 20892, USA

² National Institute of Biomedical Imaging and Bioengineering, National Institutes of Health, Bethesda, MD 20892, USA

³ Mechanobiology Institute, National University of Singapore, 117411 Singapore

The power of fluorescence microscopy to study cellular structures and macromolecular complexes spans a wide range of size scales, from studies of cell behavior and function in physiological 3D environments to understanding the molecular architecture of organelles. At each length scale, the challenge in 3D imaging is to extract the most spatial and temporal resolution possible while limiting photodamage/bleaching to living cells. Several advances in 3D fluorescence microscopy now offer higher resolution, improved speed, and reduced photobleaching relative to traditional point-scanning microscopy methods. We discuss a few specific microscopy modalities that we believe will be particularly advantageous in imaging cells and subcellular structures in physiologically relevant 3D environments.

The challenges of 3D imaging

Imaging cells and subcellular structures in 3D environments brings with it challenges that are not unique in biological microscopy, but are amplified relative to the 2D imaging of cells adhered to traditional glass coverslips *in vitro*. We will review a few of the major challenges for 3D and time-lapse 3D (4D) biological imaging, and discuss the weaknesses of conventional laser-scanning confocal microscopy in meeting these challenges. We then cover the strengths and weaknesses of newer microscopy modalities that have successfully addressed these challenges in recent years (see [Glossary](#) for an introduction to terminology).

The 3D point spread function (PSF) and imaging in thick specimens

The first and most obvious challenge of 3D imaging is that in conventional, uni-axial microscopy arrangements, the resolution along the Z-axis of the microscope is substantially (~two-fold) worse than in the lateral dimensions due to the inherent shape of the PSF ([Glossary](#); [Box 1](#) and [Figure 1](#)). The characteristic anisotropy of the PSF is seen as 'Z-stretch' in X-Z projections of reconstructed 3D image sets obtained with uni-axial fluorescence microscopy. This reduced axial resolution and Z-stretch can introduce profound errors in the tracking of objects in 4D and in colocalization in multichannel 3D imaging [1].

Adding to the problem of axial resolution is that structures of interest are sometimes tens or hundreds of

Glossary

2PM (two-photon microscopy): utilizes the near simultaneous absorption of two low-energy photons by a fluorophore, resulting in a fluorescence intensity that depends quadratically on the excitation intensity. Often employs a femtosecond pulsed laser as an illumination source. The wavelength of the two photons is roughly twice that of single-photon absorption/excitation, but can occur over a range of wavelengths. See [72] for an excellent discussion of two-photon absorption.

4Pi: a microscopy technique where diametrically opposed objective lenses are focused on the same sample plane. It is named 4π or 4Pi because unlike the partially spherical (solid angle of 2π) wavefront collected from a single objective, two opposing objectives can capture a nearly completely spherical wavefront of a solid angle of 4π . Likewise, if coherent excitation beams are delivered through the opposing lenses such that they constructively interfere at the focal plane, axial resolution may be improved by three- to sevenfold relative to microscopes with single objectives.

CCD (charge-coupled device): uses the photoelectric effect to generate electrons from photons that strike a layer of photoactive silicon, and transfers them to a capacitor array to comprise pixels, which are 'read out' in lines. Because the array is 2D, a wide-field image plane can be captured rapidly (10–20 MHz). The pixel size of most current CCD cameras varies between $3\ \mu\text{m}$ and $20\ \mu\text{m}$. EM-CCDs are electron-multiplying CCDs which have on-chip signal amplification that effectively eliminates the effect of read noise, and better sensitivity than conventional CCDs.

CLSM (confocal laser-scanning microscopy): uses a single diffraction-limited spot scanned in X and Y dimensions to excite fluorophores, and an adjustable pinhole to block out-of-focus fluorescent emission from fluorophores above and below the plane of focus.

CMOS (complementary metal-oxide-semiconductor technology): this is used in wide-field imaging detectors. Offers much faster read-out than CCD-based imaging devices, but typically at a lower quantum efficiency, greater read-noise, and higher pixel-to-pixel nonuniformity.

iPALM (interferometric photoactivated localization microscopy): uses a 4Pi geometry and single-photon interferometry for enhanced signal collection and better axial localization precision than single-objective-based PALM or STORM.

Isotropic resolution: the resolution of a microscope system with a PSF that has the same extent in all three dimensions.

LSFM (SPIM, DSLM): light-sheet-based fluorescence microscopy (including selective plane illumination microscopy and digital scanned laser light-sheet fluorescence microscopy). Uses 'sheets' of excitation light delivered to the sample in an axis orthogonal to the imaging axis.

PA-FP (photoactivatable fluorescent proteins): photoactivation generally occurs by absorption of short-wavelength light by a fluorescent protein, which allows the otherwise poorly excited fluorescent species to convert to an efficiently excited fluorescent conformation. 'Photoconvertible' proteins are similar, but shift their emission wavelength upon conversion with short-wavelength light. In the text, we use PA-FP to refer both to photoconvertible and photoactivatable proteins.

PALM (photoactivated localization microscopy): photoactivation is used to repetitively activate sparse subsets of molecules that are separated by distances larger than the diffraction limit; subsequent localization of each fluorescent emission results in a super-resolution image.

Photobleaching: the irreversible quenching of fluorescence, often due to the reaction between the excited fluorophore and oxygen. Such a reaction may also release reactive oxygen species, which can lead to further damage to other molecules in the vicinity of the dye.

PMT (photomultiplier tube): a light detector that uses the photoelectric effect to generate voltage from a detected photon, and then multiplies this voltage as much as 10^8 -fold. Used as a 'point-detector' for collecting photons from a single spatial location. In their standard configuration in CLSM microscopes they have relatively low QE (10–15%), but are very fast. PMTs can be run in

Corresponding authors: Fischer, R.S. (fischerr2@nhlbi.nih.gov); Waterman, C.M. (watermancm@nhlbi.nih.gov).

Glossary (Continued)

'photon-counting mode', which can raise the QE substantially, but this requires voltage resets after each detection event, decreasing the speed dramatically.

PSF (point spread function): the 3D diffraction pattern of a point source viewed through an objective lens.

QE (quantum efficiency): the probability that photons interacting with a detector generate electrons. QE is wavelength-dependent and can vary greatly for a given detector at different wavelengths. Current CCD cameras usually are most efficient (~60–90%) between 450 nm and 650 nm, but drop off substantially over 700 nm.

SDCM (spinning-disk confocal microscopy): uses an array of pinholes on a rapidly spinning disk that revolves on a much faster timescale than the image acquisition rate, parallelizing confocal imaging and enabling optical sectioning at a much faster rate than CLSM.

SIM (structured illumination microscopy): uses structured excitation light to generate Moiré fringes between the object and illumination pattern, thus enabling otherwise uncaptured high-frequency information to be collected by the objective and computationally resolved in Fourier space.

SNR (signal-to-noise ratio): we use this term here to mean the ratio of fluorescent signal originating from a region of interest to the total noise (resulting from Poisson statistics and imaging system/detector).

Spherical aberration: the differential focusing of light along the optical axis of a lens such that rays parallel to the optical axis but at different radial distances from the axis do not form a perfect focal point in space. Present to some extent with all spherical lenses, but is worsened when the index of refraction changes between lens, immersion media, and sample.

STORM (stochastic optical reconstruction microscopy): as with PALM, this technique uses repetitive cycles of activation and localization to assemble a super-resolution image.

micrometers away from a coverslip or objective lens front element. Focusing at these depths requires longer working distances for objective lenses, and this comes at the cost of lowering the numerical aperture, thus light collection efficiency and resolving power are reduced. Furthermore, for fluorescence techniques, excitation light penetration in most biological samples is problematic due to photonic interaction with the sample, resulting in elastic scattering [2,3]. The emitted light from a fluorophore also scatters within the sample, and thus contributes to out-of-focus fluorescence and background signal, thereby decreasing the image signal-to-noise ratio (SNR) [4]. In addition, at deeper focal planes in scattering samples, the observed PSF can degrade rapidly due to spherical aberration such that it becomes severely asymmetric along the Z-axis (Figure 1). Refractive index mismatches between thick specimens, glass, and immersion media further add to spherical aberration, inducing errors in Z localization [5].

Photobleaching and speed

Another challenge for 3D fluorescence imaging, particularly over time (4D imaging), is that excessive light exposure to the sample is inherent in the need to collect several Z-planes for each time-point, leading to problems with photobleaching of fluorophores, phototoxicity, and a slow 3D frame-rate. Photobleaching and phototoxicity occur primarily because high-energy electrons in excited fluorophores do not inevitably emit energy as fluorescence, and can instead react with dissolved oxygen. This irreversibly bleaches the fluorophore and produces highly reactive oxygen species (ROS) that cause phototoxic effects directly proportional to their diffusion and concentration. Although ROS are a major contributor to phototoxicity, other ROS-independent photodamage may also occur, leading even small amounts of light absorption to produce toxicity and unintended effects on cell function [6–8]. Although photobleaching and phototoxicity can be abrogated in part by the

Box 1. Comparison of 3D images of a point source with different imaging modalities

A 3D image of a diffraction-limited point spread function (applies to wide-field epifluorescence, confocal, two-photon, and light-sheet microscopies). Once excited, a fluorophore behaves as a point source of light. When collected by a microscope, the spread of the light waves from the point forms a diffraction pattern (Figure 1a). At high magnification in the image plane, the pattern has a central spot, the Airy disk, and diffraction rings around it. The size of the Airy disk is given by the equation

$$d = 1.22 \lambda / NA \quad [1]$$

where d is the diameter of the Airy disk, λ is the wavelength of light, and NA is the numerical aperture of the objective lens (which is determined by the index of refraction of the immersion medium and the maximum angle of light cone that can enter the lens). Thus, the higher the NA, the smaller the Airy disk becomes. The size of this Airy disk (defined as the distance between first intensity minima) limits the ability of the microscope system to resolve two point sources emitting at the same time.

Above and below the focal plane, the light spreads out from the point source, and the extent of this in 3D is known as the point spread function (PSF). When viewed perpendicular to the axis of imaging (in an X-Z plane), it has a longer distribution than it does laterally (Figure 1b). An important aspect of this is that the immersion medium in which the objective lens contacts the specimen, as well as the specimen itself, both contribute to the optics of the system. Owing to differences in refractive index of the immersion medium with that of the sample, increased spherical aberration is created as one goes deeper into samples. This causes the effective PSF (and hence the light pattern produced by it) to be asymmetric in Z and the Z-stretch to become larger (Figure 1c).

addition of oxygen scavenging systems or simple antioxidants such as L-ascorbic acid [9], the effects of phototoxicity are cumulative and directly proportional to excitation light intensity and total photon load [7]. Thus, strategies to maximize light collection efficiency and minimize excitation of the total sample volume (e.g. [6,10]) are crucial in advancing 4D imaging.

In addition to photobleaching and phototoxicity, the need to collect several Z-planes increases the acquisition time for each time-point, thus slowing the rate of 4D image acquisition. This leads to trade-offs between time resolution, imaged volume, Z-resolution, and length of imaging period, and places further constraints on the total photon load. This is particularly true with some types of very dynamic processes such as rapid cell migration, membrane remodeling or microtubule dynamics that require both high temporal and spatial resolution in 4D for motion-tracking analyses.

Limitations of scanning microscopy

Point-scanning methods such as CLSM and two-photon microscopy (2PM) have been a major boon to biological microscopy for decades, revolutionizing our ability to define the 3D structure of cells, tissues and whole animals. By rejecting out-of-focus fluorescence with a pinhole or limiting excitation to a diffraction-limited volume, CLSM and 2PM offer excellent optical sectioning because only fluorescence emitted from the diffraction-limited volume in the focal plane can reach the photomultiplier tube detector (PMT; [4] for review).

Despite their advantages and major contributions to 3D imaging, these traditional scanning techniques are

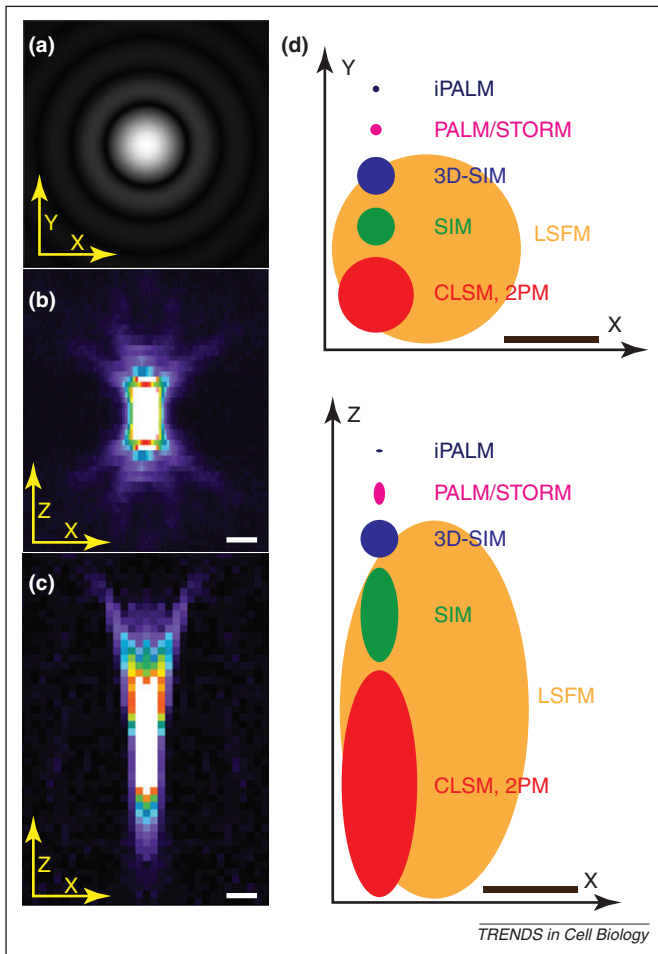


Figure 1. The effect of diffraction on imaging in 3D. (a) An idealized diffraction pattern of a point source observed in a microscope. The inner spot is the so-called Airy disk. (b) A slice in the X-Z plane from a 3D image stack of a fluorescent bead collected in an aqueous medium, centered at 5 μm from the coverslip. Note that side flanges on the distribution are symmetric in X and in Z. (c) A similar X-Z plane to that shown in (b), but taken from a 3D image stack of a fluorescent bead collected in a collagen gel at 150 μm from the coverslip. Note elongated distribution and asymmetry in the Z axis. (d) Effective PSFs of various microscopy methods, in lateral dimensions (X-Y, top) and axial dimensions (X-Z, bottom). The observed PSF of each is drawn to scale; scale bar, 0.25 μm . For super-resolution techniques, practical 'resolution volumes' are shown instead because these techniques are not limited by the diffraction-limited PSF of the microscope system.

particularly poor at overcoming the challenges to 4D imaging discussed above. First, neither CLSM nor 2PM point-scanning methods abrogate the axial stretch of the PSF discussed above (Box 1). Second, because these methods raster the excitation and detection to build an image one voxel position at a time over the entire X-Y-Z imaged volume, they suffer from slow 3D frame-rates and excessive light exposure to the specimen. This contrasts with traditional transmitted light and wide-field epifluorescence modes in which entire X-Y focal planes are imaged, reducing image frame-rate considerably for 4D imaging. Furthermore, because PMT detectors used in CLSM and 2PM are noisy and have poor quantum efficiency (QE; $\sim 10\text{--}15\%$), for sufficient fluorescence photons to reach the detector in dim or highly scattering samples, either the scan speed must be lowered to allow longer excitation dwell times, or the intensity of the excitation must be increased to accumulate more fluorescence signal [11]. Typically, the

combined effects of scanning and PMT properties result in a SNR that is several times lower than other imaging modalities [12]. Furthermore, the need to increase excitation intensity can result in fluorophore saturation [13]. In this regime, the number of fluorescent photons produced does not increase as excitation input increases, but the likelihood of triplet-state ROS production continues to increase [8]. In addition, for CLSM, although fluorescence emission collection is limited to the in-focus image volume, the entire Z-axis of the specimen is exposed to excitation throughout scanning. Coupled with the fact that peak excitation intensity with CLSM is relatively high at $\sim 1 \text{ mW}/\mu\text{m}^2$, CLSM can cause extensive photodamage and photobleaching in 4D imaging.

In 2PM the volume of excitation is restricted to a diffraction-limited region within the specimen where the pulsed long-wavelength laser intensity is high enough to produce fluorescence excitation via the non-linear two-photon effect (Figure 2) [14]. The use of long-wavelength illumination improves penetration of the sample and the limited excitation volume eliminates photobleaching in out-of-focus areas of the specimen. In addition, pulsed lasers allow second-harmonic generation imaging of collagen fibers and other non-centrosymmetric polymers without sample labeling [15–17]. Despite these advantages over CLSM, the photobleaching rate during two-photon excitation increases at a much faster rate with excitation intensity than it does with single-photon excitation [18]. Furthermore, the maximal rate at which fluorescence can be emitted from a single fluorophore is lower with two-photon excitation than with single-photon excitation [19]. Even more importantly, phototoxicity observed with two-photon excitation may actually be worse than with single-photon excitation in some cases [19,20]. Although the average power of the input beam over time may be relatively low, the instantaneous power during an excitation pulse can be as high as $10 \text{ W}/\mu\text{m}^2$ [11]. Nevertheless, because of its ability to limit excitation volume and penetrate deep into tissues, 2PM will continue to be a primary tool for 3D and 4D imaging, particularly intravital in adult animals [21–23]. Furthermore, 2PM will be particularly advantageous if used in conjunction with other optical sectioning techniques (discussed below) [24,25].

Solutions for 3D imaging

Breaking the resolution barrier: super-resolution in 3D

The most fundamental challenges to 3D optical imaging are the resolution limit imposed by diffraction and the anisotropic nature of the PSF, which reduces resolution in the axial dimension compared to the lateral dimensions. These challenges have been overcome recently by structured illumination microscopy (SIM) as well as point-source localization techniques that hold great promise for the future.

SIM

Although optical sectioning of 3D samples is most often obtained through either CLSM or 2PM, optical sectioning can also be performed using a wide-field microscope with laterally structured illumination [26]. SIM was first introduced to enhance lateral resolution beyond the limits of

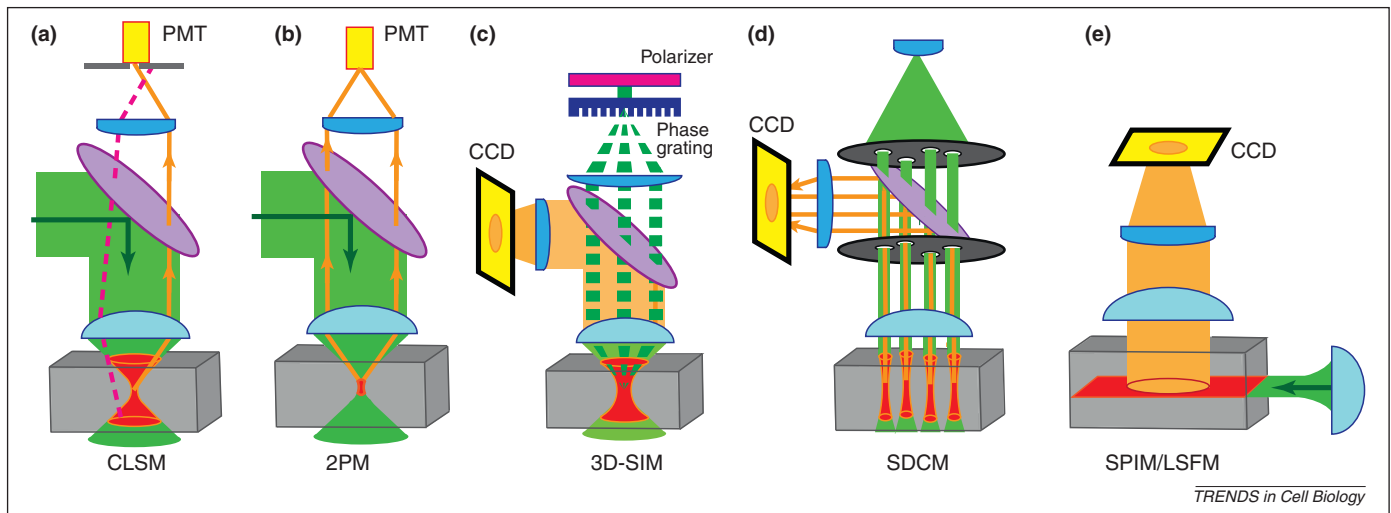


Figure 2. Optical paths of 3D microscopy modes. In all panels, illumination light is green, dichromatic mirror is purple, specimen is grey, sample excitation is red, in-focus fluorescence emission is orange, lenses are blue, detector is yellow. **(a)** Confocal laser-scanning microscopy light path. Excitation laser light is focused through the objective lens to a diffraction-limited spot in the focal plane of the sample. Note that fluorescence is excited above and below the focal plane. Out-of-focus fluorescence (pink) is rejected by the pinhole, while in-focus light is allowed through the pinhole (black) and collected by the photomultiplier (PMT). **(b)** Two-photon microscopy light path. Infrared pulsed-laser illumination is focused to a diffraction-limited volume such that two-photon excitation is confined to this small volume (red). Because all fluorescence created by this excitation originates in the focal plane, no pinhole is needed, and all fluorescence captured by the objective lens is focused to the point source detector (PMT). **(c)** Structured illumination microscopy. Laser illumination is collimated onto a phase grating, creating three alternative phases that are recombined through the objective lens into the sample where they interfere to create 3D patterned illumination. Because excitation over all collected phases is essentially equivalent to wide-field excitation, the entire axial volume is excited. Resulting fluorescence from each phase collection is reflected by the dichroic mirror and detected by a CCD. **(d)** Spinning-disk confocal microscopy light path. Laser excitation light passes through dual pinhole-array disks (black) that scan the excitation across the specimen by spinning at high speed. The fluorescence from points in the focal plane pass through the proximal disc pinholes, and are reflected by a dichroic mirror to an array detector such as a charge-coupled device (CCD) camera. For clarity, only four pinhole paths are shown. The sum of all scanning pinhole illumination over time excites the full axial volume of the sample. **(e)** Light-sheet fluorescence microscopy light path. Excitation light is focused into a sheet that is delivered to the specimen orthogonally to the axis of imaging. Thus, only the plane of focus is excited. Because all fluorescence is from the focal plane, no pinhole is needed, and the field of fluorescence is collected by an array detector, such as a CCD camera.

diffraction [27–29]. In SIM, the sample is illuminated with patterned light, producing Moire fringes or a ‘beat pattern’ that moves otherwise unresolvable high-frequency information into the passband of the microscope objective. By taking multiple images with phase-shifted patterned illumination, it is possible to remove the excitation pattern computationally and reassemble an image with approximately twice the resolution of the original images.

Gustafsson and coworkers expanded the initial 2D technique by using three mutually coherent beams to generate interferometrically patterned excitation in both axial and lateral dimensions [28], offering resolution doubling in all three dimensions (Figure 2). This version of 3D-SIM can be improved further by employing two opposed objective lenses in a ‘4Pi geometry’ and a beam splitter that makes six coherent beams [30]. In the 4Pi implementation, the resultant images do not suffer from the same Z-stretch observed with confocal images [28,30,31] and ~100 nm near-isotropic resolution is obtained. In addition to the significant increase in resolution, 3D-SIM does not rely on a pinhole, thus enabling efficient light collection, good sensitivity, and the ability to capture wide-field images on a high-QE, low-noise array detector such as charge-coupled device (CCD) or complementary metal-oxide semiconductor (CMOS) cameras. In addition, SIM is relatively easy and inexpensive to implement in the context of a traditional wide-field epifluorescence microscope, and several manufacturers already have commercialized 2D-SIM systems on the market. The power of SIM to study processes in cells in 3D has been beautifully demonstrated in the analysis of nuclear structure and chromatin organization

[32], and the dynamics of the cell cortex at the cytokinetic furrow [33,34].

Although SIM holds much promise for future studies of cells and cellular architecture in 3D below the diffraction barrier, several caveats apply. First, because multiple exposures with varying phase need to be captured for each Z-plane (15 for 3D-SIM), SIM has intrinsic speed limitations. Although increases in camera sensitivity and speed have enabled live cells to be studied with high spatial and temporal resolution using 2D-SIM, movements of structures by more than one resolution length in the time it takes to acquire the requisite phased images result in image reconstruction artifacts [35]. 2D-SIM can be performed at relatively high speeds (up to 11 Hz), but multi-color 3D-SIM is more practical at speeds of one Z-plane every 2–6 seconds [6,32]. For 3D applications this is an important limitation to consider when one is studying dynamic processes. Second, although SIM effectively removes out-of-focus light computationally, it still leaves behind the associated shot noise [28]. Thus, in practice, in very thick samples with a large amount of out-of-focus light, 3D-SIM may produce lower contrast images compared to confocal approaches. Finally, current implementations of 3D-SIM rely on interferometric pattern generation, and therefore very thick or highly scattering samples will probably degrade the pattern enough that reconstructions will suffer. Future use of non-linear optics with 3D-SIM may extend its useful working distance and reduce photobleaching through the volume of the specimen. In any case, because of its relatively inexpensive implementation on existing microscope platforms and

greatly improved resolution, 3D-SIM will probably contribute to important advances in understanding organelle structure and function within cells.

STORM and PALM in 3D

Another group of approaches that overcomes the limitations of diffraction are the ‘pointillist’ super-resolution localization techniques including (fluorescence) photoactivated localization microscopy, (f)PALM [36,37] (referred to henceforth as PALM), and stochastic optical reconstruction microscopy, STORM [38], which in some cases offer localization precision of less than 20 nm. These techniques rely on iterative cycles of activation, excitation and photobleaching coupled with image acquisition, and subsequent localization with subdiffraction accuracy of small numbers of labeled molecules that are separated in space by greater than the Rayleigh limit within a densely labeled specimen (Figure 3). To achieve spatially separated

excitation/emission events, PALM uses genetically photoswitchable fluorescent proteins to switch between emission wavelengths or between a dark and fluorescent state [39], whereas STORM utilizes reducing buffers and small-molecule fluorophores to similar effect [40]. Localization in both cases is achieved by fitting the image of individual molecules to a model PSF [41], computing its centroid [42], or by performing a cross-correlation to an experimental PSF [25]. Because localizations of many isolated fluorophores are collected over hundreds to many thousands of frames to build up a localization image of fluorophores at high density, PALM images are typically acquired in a few tens of seconds to tens of minutes.

PALM and STORM have been extended to the third dimension, either by optically altering the shape of the PSF as a function of axial depth [40,43] or by simultaneous collection of two planes to collect 3D data which are fit to a 3D PSF [37], thereby enhancing subdiffraction localization capability along the Z-axis. In STORM, use of a cylindrical lens in the optical path creates controlled astigmatism to distort the PSF as a function of Z position (Figure 4a) [40,43]. By comparing the PSF of a fluorophore to a calibration, a localization precision of ~50–100 nm in the Z direction can be achieved over an axial range of several micrometers. This approach has enabled the first super-resolution images of the clathrin-coated pit structure [40,44,45]. However, imaging thicker 3D samples is difficult because conventional wide-field illumination activates and excites many out-of-focus probe molecules, increasing background and impeding the isolation of single molecules in the imaging plane. Out-of-focus activation and excitation has the additional disadvantage that it potentially wastes localizations, decreasing the effective label density and reducing image resolution. Use of two-photon activation [46] in ‘3D-PALM’ can be used to avoid this problem by limiting photoactivation to the focal plane, and has been demonstrated up to ~8 μm deep in the sample while retaining high localization densities [25]. Future technical improvements may better confine the illumination, extending the per-molecule photon budget and permitting 3D super-resolution at greater depths.

For 3D imaging of samples up to ~300 nm in thickness, interferometric photoactivated localization microscopy (iPALM) offers unmatched localization precision. iPALM uses localization of single molecules for super-resolution in the lateral (X–Y) dimension, and simultaneous multiphase interferometry for super-resolution in the axial (Z) dimension. Similarly to its 2D counterparts, iPALM depends on photoswitching of small populations of fluorophores to determine X–Y coordinates (Figure 3). However, in iPALM the enhanced resolution along the Z-axis is achieved by using dual objectives in an opposed, 4Pi configuration (Figure 4), thus allowing each emitted photon to propagate through both top and bottom objectives and be recombined in a beamsplitter. The optical path-length difference between the top and bottom emission beams, and hence the phase of the recombined signal, is directly proportional to the Z coordinate (Figure 4b). Due to the greater collection efficiency of the 4Pi geometry in iPALM, X–Y localization precision is typically higher than in conventional PALM. In addition, the high sensitivity afforded by interferometry

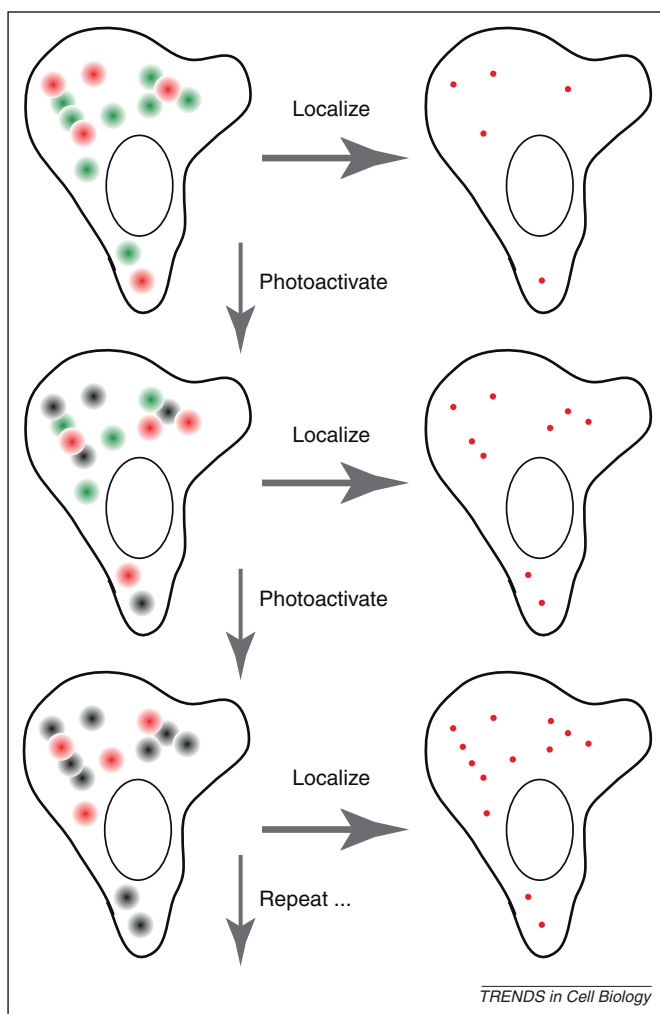


Figure 3. Photoactivated point source localization. In PALM and STORM, cells express proteins tagged with photoactivatable or photoconvertible fluorophores (green), random subsets of which are converted to fluoresce (red). Each of these single-molecule point sources creates an Airy disk-like distribution of fluorescence at the detector, and the center of each such distribution is found computationally (red points in cell image on right). Because the molecules in the random subset are separated in space, overlap of the fluorescent emissions does not occur. Each fluorophore is imaged until it bleaches (grey), and then a new round of photoconversion and excitation occurs. As the cycles continue, point sources are imaged, localized, and bleached to build a dense localization map (bottom right).

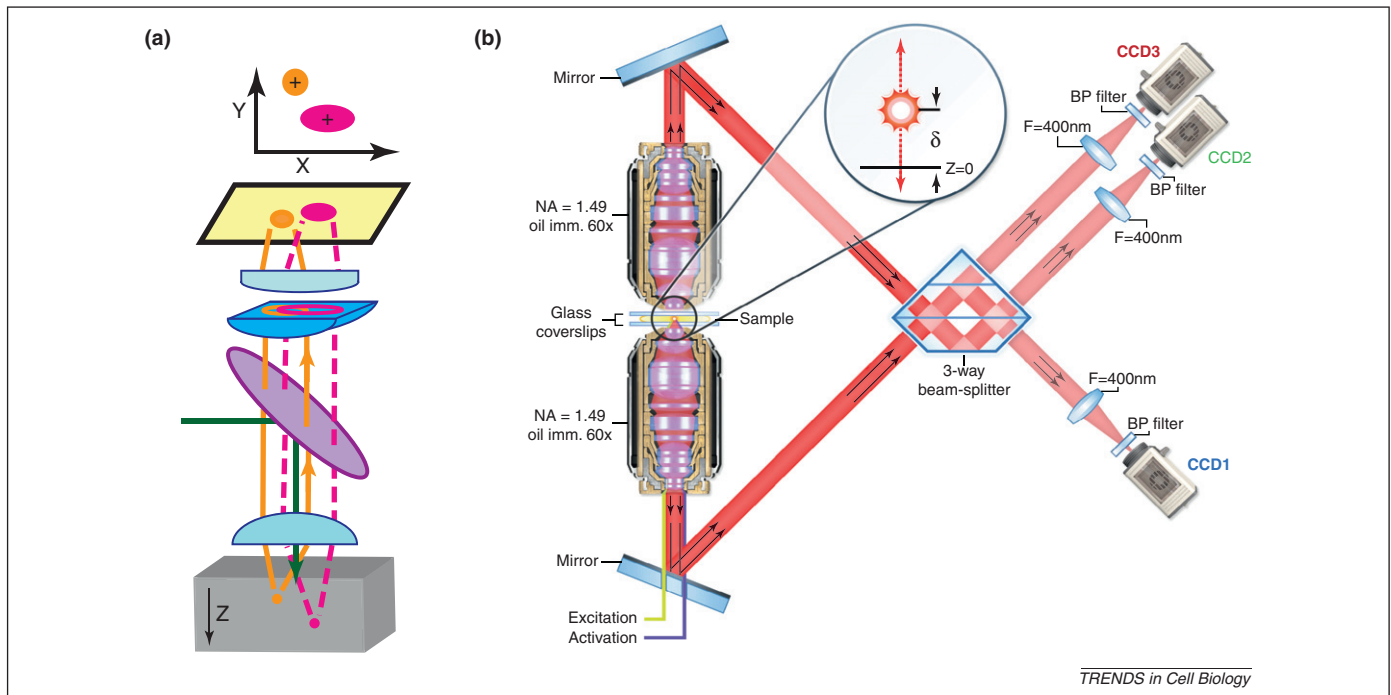


Figure 4. 3D super-resolution microscopy approaches. (a) 3D-PALM/STORM. Small subsets of molecules are activated to fluoresce, isolated in space and time enough that they can be captured as distinct point sources. A weak cylindrical lens is inserted into the optical path (dark blue), which creates astigmatism such that point sources in the center focal plane (orange) appear to be laterally symmetric, whereas point sources at other Z-planes (pink) are distorted in either the X or Y direction (depending on depth), to appear elliptical on the CCD detector. Using known calibration curves of point sources enables Z-localization below the diffraction-limited resolution based on the shapes of the point sources observed in the image. (b) iPALM. Opposed high numerical aperture objective lenses are used to collect fluorescent light waves from photoactivated fluorescent point sources. Because a given fluorophore emits in all directions, both objectives capture the fluorescence, but the difference in the path traveled by each portion of the emitted fluorescence wave depends on the Z-plane of the original point source. The collected fluorescence is recombined with a three-way beam splitter, which causes self-interference of each fluorescent photon. Such interference creates different intensities in the three output beams from the beam splitter, which vary according to the path-length differences in the axial direction. Measurement of the relative intensities across the three detectors enables axial resolution better than 20 nm. Panel (b) was reprinted with permission from [47].

can result in an axial localization precision better than 10 nm [47]. Indeed, in iPALM, axial resolution is approximately two-fold better than the lateral resolution, unlike single-objective-based techniques where axial resolution is typically two- to threefold worse than lateral resolution. Owing to the high resolution, iPALM is thus advantageous for investigating molecular organization at the ultrastructural level. For example, iPALM was deployed to study focal adhesions [48], integrin-based adhesive organelles that play important roles in cell migration, matrix remodeling, and mechanotransduction. Because of their density and complex composition, molecular organization within focal adhesions has long been difficult to access by techniques such as electron microscopy (EM). iPALM revealed for the first time that focal adhesion proteins are stratified along the axial dimension, and was used to deduce the molecular orientation of talin within these structures [48].

Although iPALM provides a high spatial resolution approaching that of EM, several limitations remain. Because direct optical access is required from both sides, the sample must be relatively thin (less than 15–20 μm). Similarly, the axial range of imaging depth is limited to ~ 250 –600 nm [47]. Also, iPALM instrumentation is technically complex and demands very high mechanical and thermal stability. By contrast, the instrumentation for conventional PALM and STORM (Figure 4a) is relatively simple, free localization software [42] is available, and

several major manufacturers now offer turnkey commercial platforms with some 3D capability (based on biplane imaging and astigmatism) that are compatible with suitable dyes, making these technologies even more accessible. Although PALM and STORM offer superb resolution for 3D imaging, the need to collect hundreds to tens of thousands of raw frames for a single reconstructed image places a severe limitation on the imaging speed. Progress in dye brightness, contrast and attachment chemistry [49] suggests that the field will continue to evolve, with the promise of faster live cell applications, in multicolor and 3D [50]. Despite of their limitations in speed, PALM, STORM and iPALM offer near-ultrastructural 3D resolution together with the molecular specificity of fluorescent labeling, and will continue to answer important questions about molecular-scale biological architecture that have eluded electron imaging-based approaches.

Breaking the speed limit: spinning disks to light sheets

Another major set of challenges for 4D imaging has been the inherent speed limitation of point-scanning techniques for optical sectioning, together with the photobleaching that accompanies 4D imaging, as discussed above. Two basic approaches have been used to address these challenges: multiplexing of confocal pinholes, such as in spinning-disk confocal microscopy, and use of orthogonal plane illumination in light-sheet fluorescence microscopy.

Spinning-disk confocal microscopy (SDCM)

Several methods have been developed for taking advantage of the confocal principle of pinhole-based out-of-focus light rejection while maintaining the ability to generate wide-field images to overcome the speed limitations of point-scanning microscopy. These include slit scanning [51] and pinhole multiplexing methods, including swept-field and spinning Nipkow disk confocal techniques. Of these, the most robust method that has gained wide acceptance among biologists is SDCM. This method uses an array of excitation and emission pinhole apertures on a rapidly spinning disk, such that the pinhole array sweeps the entire field of view over 1000 times per second (reviewed in [52]). The high scan speed not only improves image acquisition rate (up to 360 frames per second [53]), it also has the effect of lowering the peak excitation light density down to a few $\mu\text{W}/\mu\text{m}^2$, thereby increasing fluorescence efficiency and decreasing photobleaching and photodamage effects compared with point scanning [13]. Perhaps most importantly, because the entire confocal field of view can be captured by a high-QE, low-noise camera instead of a PMT, SDCM systems have more than 50-fold increase in light capture efficiency, resulting in a several-fold increase in SNR relative to CLSM or 2PM [12,13]. Because of these advantages, SDCM has been well-suited to the study of cells in 3D extracellular matrices [54], engineered tissue in matrices [55], as well as intravital imaging [56,57]. The ability to rapidly collect entire frames at once also enables the quantitative study of very dynamic processes, such as microtubule dynamics in cells in 3D matrices [58].

Although SDCM has many powerful features for 4D imaging, there are a few caveats and limitations. First, as with other linear excitation imaging methods, SDCM suffers from problems with illumination penetration of the sample and photobleaching of the entire axial column of the specimen at each Z-plane for each time-point. Second, imaging thick specimens suffers from an effect known as 'pinhole crosstalk'. Because light emitted from a point in a focal plane expands over distance, portions of this light can enter adjacent pinholes, and scattering of light in the sample increases this effect. Third, because pinhole size is fixed in current implementations of SDCM, this limits its use to high-magnification, high-resolution objective lenses. Finally, SDCM suffers from the same axial resolution problems of other confocal methods (Table 1). However, because of its high speed, low noise and reduced photobleaching compared to CLSM, SDCM will continue to be extremely important for imaging fast cell and organelle dynamics in 3D.

Light-sheet-based fluorescence microscopy (LSFM)

In LSFM [59], known in different implementations as 'selective plane illumination', SPIM [60], or 'digital scanned laser light-sheet fluorescence microscopy', DSLM [61], the sample is illuminated with a thin sheet of light from the side of the specimen to illuminate a single X-Y plane, and widefield fluorescence detection takes place in the direction perpendicular to excitation (Figure 2). This geometry leads to major advantages over confocal and two-photon approaches. First, acquisition speed is greatly

increased relative to point-scanning methods because the entire imaging plane is detected simultaneously. A volume is recorded by scanning the light sheet in the axial dimension, instead of the 3D scan required for point scanning. Second, excitation is confined to the focal plane, providing optical sectioning without pinholes, thus boosting detection efficiency while reducing photobleaching and photodamage to rates far below those encountered with other techniques. Finally, because acquisition is parallelized, each pixel is exposed for the full integration time of a high-QE, low-noise wide-field camera, resulting in ~ 10 –1000-fold higher SNR than point-scanning techniques operating at similar frame-rates.

The high SNR and very fast acquisition afforded by LSFM have enabled ground-breaking observations of vertebrate embryonic development [60,62,63] and photomanipulation of cardiac pace-making function *in vivo* [64]. Improving the axial resolution of LSFM by using a Bessel beam and structured illumination (discussed below) has provided high-speed, isotropically resolved 4D imaging of cellular dynamics [24]. 3D cell culture can likewise be imaged over long times using LSFM [65].

In spite of these advantages, LSFM does possess drawbacks compared to other 4D imaging techniques. First, the axial range of LSFM is reduced compared to 2PM because the effect of scattering degrades the excitation sheet and is more pronounced on the emission side due to wide-field detection. Using a femtosecond laser for two-photon light-sheet excitation mitigates some of this disadvantage, providing an interesting hybrid technique that combines advantages of 2PM and LSFM [66]. Second, the spatial resolution of LSFM is generally lower than other techniques, which is why most applications have targeted larger systems such as whole embryos or tissue slices [60–62,67], instead of single cells. Lateral resolution is determined by the numerical aperture (NA) of the detection lens, whereas axial resolution is determined by both the detection objective and the light-sheet thickness. The perpendicular excitation/detection geometry required by LSFM forces the use of long working distance, somewhat low NA (typically 1.0 or less) objective lenses. In almost all LSFM implementations, the light sheet is created from a Gaussian beam. Gaussian beams undergo widening at increasing distances from the beam waist, coupling the quality of optical sectioning to the position within the field of view and degrading the effective axial resolution at the sample edges. Exciting a fluorescent sample with a scanned Bessel beam [68] in an LSFM geometry mitigates this problem and improves axial resolution [24]. Such a resolution improvement comes at a cost, however, because 'side lobes' in the excitation profile cause significant out-of-plane illumination. Removing the contaminating effects of the side lobes requires either structured illumination or two-photon excitation. Finally, implementing LSFM is nontrivial, thus despite its exceptional promise, until LSFM becomes commercially available it is likely to remain the province of relatively few labs. However, once commercialized, LSFM promises to be extremely important for imaging cellular dynamics in larger, thick specimens such as whole animals during early development.

Table 1. Practical comparison of several 3D microscopy modes

Mode	Best-suited applications	Advantages for 3D biology	Limitations	Practical imaging depth (μm)	Resolution	Commercially available	Refs
CLSM ^a	Cell structure analyses <i>in vitro</i> and <i>in vivo</i> with bright, fixed samples, live cell FRAP analysis	Widely available, 2D ROI photomanipulation, good axial sectioning performance	High photobleaching and photodamage Slow speed in 4D, poor SNR	200	250 nm XY, >600 nm Z	Yes	[4]
2PM	intravital imaging, SHG imaging of collagen and fluorescence together, bright samples	3D ROI photomanipulation, SHG, deepest sample penetration	Nonlinear photodamage Slow speed in 4D, pulsed lasers expensive, poor SNR	600–800	250 nm XY, >600 nm Z	Yes	[14,15, 72–74]
SDCM	High resolution live cell and organelle dynamics, cyoskeletal and membrane dynamics, dim samples (FSM)	Widely available, high speed, good SNR with good CCD camera, high sensitivity	Pinhole crosstalk, no ROI control No low magnification imaging	150	250 nm XY, >600 nm Z	Yes	[53,56, 75–77]
LSFM	Whole cell dynamics during embryo development or other long time scale dynamics, cell surface dynamics with Bessel beam (e.g. filopodial dynamics on single cells)	Very high speed, very low photodamage, good SNR, higher resolution possible combined with 2P, Bessel, SI, or DLSM excitation	No high NA objectives, poor light collection, lower resolution, sample mounting issues	200–500	500 nm XY, 1–3 μm Z; 300 nm X,Y,Z for Bessel	No	[24,59, 62,64, 66,67]
3D-SIM	Macromolecular assemblies and organelles with relatively slow dynamics (e.g. chromatin remodeling). Low scattering samples are best	Resolution $\sim 2\times$ better than diffraction-limited, light efficient	Slow speed, photodamage possible, limited imaging depth, multiple raw images needed per 3D-SIM image, shot noise not removed, complex optical configuration	20–40	100 nm XY, 250 nm Z, 100 nm XYZ in with 3D-SIM (4Pi configuration)	Yes	[6,28, 29,33, 35]
3D-STORM/ 3D-PALM	Macromolecular assemblies and organelles in fixed difficult to image by diffraction limited imaging (e.g. microbial structure, membranous vesicles)	Resolution $\sim 10\times$ better than diffraction limited, amenable to whole cell imaging, simple optical configuration	Limited imaging depth, slow speed, reducing out-of-focus activation requires either TPM or light-sheet illumination, limited subset of dyes/PA-FPs, mostly fixed cells	10	20–40 nm XY, 40–80 nm Z	Yes	[25,37, 38,42, 43,45, 46,50, 78–80]
iPALM	Cell surface-associated macromolecular assemblies and organelles with complex structure in fixed samples (e.g. membrane-bound protein complexes such as adhesion organelles, immune synapses)	Ultra-high (< 20 nm) resolution in 3D, possible to determine protein orientation or conformation change	Very limited imaging depth, slow speed, limited subset of dyes/PA-FPs, fixed samples only, complex optical configuration	0.5	10–20 nm XY, 5–10 nm Z	No	[47,48]

^aAbbreviations: CCD, charge-coupled device; CLSM, confocal laser-scanning microscopy; DLSM, dynamic light scattering microscopy; 3D-PALM, three-dimensional photoactivation localization microscopy; 3D-SIM, three-dimensional structured illumination microscopy; 3D-STORM, three-dimensional stochastic optical reconstruction microscopy; FPs, fluorescent proteins; FRAP, fluorescence recovery after photobleaching; FSM, fluorescent speckle microscopy; iPALM, interferometric photoactivation localization microscopy; LSFM, light-sheet fluorescence microscopy; NA, numerical aperture; PA-FPs, photoactivatable fluorescent proteins; ROI, region of interest; SDCM, spinning-disk confocal microscopy; SHG, second harmonic generation; SI, structured illumination microscopy; SNR, signal-to-noise ratio; TPM, two-photon microscopy.

Concluding remarks

The array of imaging modalities available for the study of animals, tissues, cells and cellular components in 3D has increased dramatically over the last decade. We have only covered a few promising modalities for 3D cell biology, but there are others that are also able to give super-resolution

images of biological processes in 3D [69], such as stimulated emission-depletion microscopy (STED), which are well-covered elsewhere [70,71]. As more of these modalities become commercially available, this will expand the imaging toolbox for a much wider audience of biologists (Table 1). As the audience broadens, more robust reagents

and components will inevitably follow. However, each imaging modality has relative strengths and weaknesses that need to be taken into account for a given biological problem; as with any technology, there is no single tool for all jobs. As in the past, the best results will be obtained when the imaging modality is ideally matched to the biological question at hand.

References

- Waters, J.C. (2009) Accuracy and precision in quantitative fluorescence microscopy. *J. Cell Biol.* 185, 1135–1148
- Cheong, W. *et al.* (1990) A review of the optical properties of biological tissues. *IEEE J. Quantum Electron.* 26, 2166–2185
- Ntziachristos, V. (2010) Going deeper than microscopy: the optical imaging frontier in biology. *Nat. Methods* 7, 603–614
- Conchello, J.A. and Lichtman, J.W. (2005) Optical sectioning microscopy. *Nat. Methods* 2, 920–931
- Egner, A. *et al.* (1998) Refractive index mismatch induced intensity and phase variations in fluorescence confocal, multiphoton and 4Pi-microscopy. *Opt. Commun.* 153, 211–217
- Carlton, P.M. *et al.* (2010) Fast live simultaneous multiwavelength four-dimensional optical microscopy. *Proc. Natl. Acad. Sci. U.S.A.* 107, 16016–16022
- Hoebe, R.A. *et al.* (2008) Quantitative determination of the reduction of phototoxicity and photobleaching by controlled light exposure microscopy. *J. Microsc.* 231, 9–20
- Stephens, D.J. and Allan, V.J. (2003) Light microscopy techniques for live cell imaging. *Science* 300, 82–86
- Knight, M.M. *et al.* (2003) Live cell imaging using confocal microscopy induces intracellular calcium transients and cell death. *Am. J. Physiol. Cell Physiol.* 284, C1083–C1089
- Hoebe, R.A. *et al.* (2007) Controlled light-exposure microscopy reduces photobleaching and phototoxicity in fluorescence live-cell imaging. *Nat. Biotechnol.* 25, 249–253
- Shaw, P.J. (2006) Comparison of widefield/deconvolution and confocal microscopy for three-dimensional imaging. In *Handbook of Biological Confocal Microscopy* (Pawley, J.B., ed.), pp. 453–467, Plenum Press
- Murray, J.M. *et al.* (2007) Evaluating performance in three-dimensional fluorescence microscopy. *J. Microsc.* 228, 390–405
- Wang, E. *et al.* (2005) Performance comparison between the high-speed Yokogawa spinning disc confocal system and single-point scanning confocal systems. *J. Microsc.* 218, 148–159
- Helmchen, F. and Denk, W. (2005) Deep tissue two-photon microscopy. *Nat. Methods* 2, 932–940
- Campagnola, P.J. and Loew, L.M. (2003) Second-harmonic imaging microscopy for visualizing biomolecular arrays in cells, tissues and organisms. *Nat. Biotechnol.* 21, 1356–1360
- Iina, O. *et al.* (2011) Two-photon laser-generated microtracks in 3D collagen lattices: principles of MMP-dependent and -independent collective cancer cell invasion. *Phys. Biol.* 8, 015010
- Wolf, K. *et al.* (2009) Collagen-based cell migration models *in vitro* and *in vivo*. *Semin. Cell Dev. Biol.* 20, 931–941
- Patterson, G.H. and Piston, D.W. (2000) Photobleaching in two-photon excitation microscopy. *Biophys. J.* 78, 2159–2162
- Hopt, A. and Neher, E. (2001) Highly nonlinear photodamage in two-photon fluorescence microscopy. *Biophys. J.* 80, 2029–2036
- Konig, K. *et al.* (1999) Pulse-length dependence of cellular response to intense near-infrared laser pulses in multiphoton microscopes. *Opt. Lett.* 24, 113–115
- Celli, S. *et al.* (2011) Visualizing the innate and adaptive immune responses underlying allograft rejection by two-photon microscopy. *Nat. Med.* 17, 744–749
- Celli, S. *et al.* (2008) Intravital two-photon imaging of natural killer cells and dendritic cells in lymph nodes. *Methods Mol. Biol.* 415, 119–126
- Roussos, E.T. *et al.* (2011) Chemotaxis in cancer. *Nat. Rev. Cancer* 11, 573–587
- Planchon, T.A. *et al.* (2011) Rapid three-dimensional isotropic imaging of living cells using Bessel beam plane illumination. *Nat. Methods* 8, 417–423
- York, A.G. *et al.* (2011) Confined activation and subdiffraction localization enables whole-cell PALM with genetically expressed probes. *Nat. Methods* 8, 327–333
- Gustafsson, M.G. (2000) Surpassing the lateral resolution limit by a factor of two using structured illumination microscopy. *J. Microsc.* 198, 82–87
- Gustafsson, M.G. (2005) Nonlinear structured-illumination microscopy: wide-field fluorescence imaging with theoretically unlimited resolution. *Proc. Natl. Acad. Sci. U.S.A.* 102, 13081–13086
- Gustafsson, M.G. *et al.* (2008) Three-dimensional resolution doubling in wide-field fluorescence microscopy by structured illumination. *Biophys. J.* 94, 4957–4970
- Hirvonen, L.M. *et al.* (2009) Structured illumination microscopy of a living cell. *Eur. Biophys. J.* 38, 807–812
- Shao, L. *et al.* (2008) I5S: wide-field light microscopy with 100-nm-scale resolution in three dimensions. *Biophys. J.* 94, 4971–4983
- Wang, L. *et al.* (2011) Wide-field high-resolution structured illumination solid immersion fluorescence microscopy. *Opt. Lett.* 36, 2794–2796
- Schermelleh, L. *et al.* (2008) Subdiffraction multicolor imaging of the nuclear periphery with 3D structured illumination microscopy. *Science* 320, 1332–1336
- Elia, N. *et al.* (2011) Dynamics of endosomal sorting complex required for transport (ESCRT) machinery during cytokinesis and its role in abscission. *Proc. Natl. Acad. Sci. U.S.A.* 108, 4846–4851
- Guizetti, J. *et al.* (2011) Cortical constriction during abscission involves helices of ESCRT-III-dependent filaments. *Science* 331, 1616–1620
- Kner, P. *et al.* (2009) Super-resolution video microscopy of live cells by structured illumination. *Nat. Methods* 6, 339–342
- Betzig, E. *et al.* (2006) Imaging intracellular fluorescent proteins at nanometer resolution. *Science* 313, 1642–1645
- Juette, M.F. *et al.* (2008) Three-dimensional sub-100 nm resolution fluorescence microscopy of thick samples. *Nat. Methods* 5, 527–529
- Rust, M.J. *et al.* (2006) Sub-diffraction-limit imaging by stochastic optical reconstruction microscopy (STORM). *Nat. Methods* 3, 793–795
- Heilemann, M. *et al.* (2008) Subdiffraction-resolution fluorescence imaging with conventional fluorescent probes. *Angew. Chem. Int. Ed. Engl.* 47, 6172–6176
- Huang, B. *et al.* (2008) Three-dimensional super-resolution imaging by stochastic optical reconstruction microscopy. *Science* 319, 810–813
- Thompson, M.A. *et al.* (2009) Localizing and tracking single nanoscale emitters in three dimensions with high spatiotemporal resolution using a double-helix point spread function. *Nano Lett.* 10, 211–218
- Henriques, R. *et al.* (2010) QuickPALM: 3D real-time photoactivation nanoscopy image processing in ImageJ. *Nat. Methods* 7, 339–340
- Huang, B. *et al.* (2008) Whole-cell 3D STORM reveals interactions between cellular structures with nanometer-scale resolution. *Nat. Methods* 5, 1047–1052
- Bates, M. *et al.* (2007) Multicolor super-resolution imaging with photo-switchable fluorescent probes. *Science* 317, 1749–1753
- Wu, M. *et al.* (2010) Coupling between clathrin-dependent endocytic budding and F-BAR-dependent tubulation in a cell-free system. *Nat. Cell Biol.* 12, 902–908
- Vaziri, A. *et al.* (2008) Multilayer three-dimensional super resolution imaging of thick biological samples. *Proc. Natl. Acad. Sci. U.S.A.* 105, 20221–20226
- Shtengel, G. *et al.* (2009) Interferometric fluorescent super-resolution microscopy resolves 3D cellular ultrastructure. *Proc. Natl. Acad. Sci. U.S.A.* 106, 3125–3130
- Kanchanawong, P. *et al.* (2010) Nanoscale architecture of integrin-based cell adhesions. *Nature* 468, 580–584
- Klein, T. *et al.* (2010) Live-cell dSTORM with SNAP-tag fusion proteins. *Nat. Methods* 8, 7–9
- Jones, S.A. *et al.* (2011) Fast, three-dimensional super-resolution imaging of live cells. *Nat. Methods* 8, 499–508
- Benedetti, P.A. *et al.* (1992) Confocal-line microscopy. *J. Microsc.* 165, 119–129
- Wilson, T. (2011) Spinning-disk microscopy systems. In *Imaging: A Laboratory Manual* (Yuste, R., ed.), Cold Spring Harbor Press, pp. 100–125
- Graf, R. *et al.* (2005) Live cell spinning disk microscopy. *Adv. Biochem. Eng. Biotechnol.* 95, 57–75

- 54 Ewald, A.J. *et al.* (2008) Collective epithelial migration and cell rearrangements drive mammary branching morphogenesis. *Dev. Cell* 14, 570–581
- 55 Grainger, S.J. and Putnam, A.J. (2011) Assessing the permeability of engineered capillary networks in a 3D culture. *PLoS ONE* 6, e22086
- 56 Ewald, A.J. *et al.* (2011) Dynamic, long-term *in vivo* imaging of tumor-stroma interactions in mouse models of breast cancer using spinning-disk confocal microscopy. In *Live Cell Imaging: A Laboratory Manual* (Goldman, R.D. *et al.*, eds), Cold Spring Harbor Press, pp. 419–431
- 57 McDonald, B. *et al.* (2010) Intravascular danger signals guide neutrophils to sites of sterile inflammation. *Science* 330, 362–366
- 58 Myers, K.A. *et al.* (2011) Distinct ECM mechanosensing pathways regulate microtubule dynamics to control endothelial cell branching morphogenesis. *J. Cell Biol.* 192, 321–334
- 59 Huisken, J. and Stainier, D.Y. (2009) Selective plane illumination microscopy techniques in developmental biology. *Development* 136, 1963–1975
- 60 Huisken, J. *et al.* (2004) Optical sectioning deep inside live embryos by selective plane illumination microscopy. *Science* 305, 1007–1009
- 61 Keller, P.J. and Stelzer, E.H. (2008) Quantitative *in vivo* imaging of entire embryos with Digital Scanned Laser Light Sheet Fluorescence Microscopy. *Curr. Opin. Neurobiol.* 18, 624–632
- 62 Keller, P.J. *et al.* (2010) Fast, high-contrast imaging of animal development with scanned light sheet-based structured-illumination microscopy. *Nat. Methods* 7, 637–642
- 63 Keller, P.J. *et al.* (2008) Reconstruction of zebrafish early embryonic development by scanned light sheet microscopy. *Science* 322, 1065–1069
- 64 Arrenberg, A.B. *et al.* (2010) Optogenetic control of cardiac function. *Science* 330, 971–974
- 65 Verveer, P.J. *et al.* (2007) High-resolution three-dimensional imaging of large specimens with light sheet-based microscopy. *Nat. Methods* 4, 311–313
- 66 Truong, T.V. *et al.* (2011) Deep and fast live imaging with two-photon scanned light-sheet microscopy. *Nat. Methods* 8, 757–760
- 67 Holekamp, T.F. *et al.* (2008) Fast three-dimensional fluorescence imaging of activity in neural populations by objective-coupled planar illumination microscopy. *Neuron* 57, 661–672
- 68 Durnin, J. *et al.* (1988) Comparison of Bessel and Gaussian beams. *Opt. Lett.* 13, 79
- 69 Urban, N.T. *et al.* (2011) STED nanoscopy of actin dynamics in synapses deep inside living brain slices. *Biophys. J.* 101, 1277–1284
- 70 Vicidomini, G. *et al.* (2011) Sharper low-power STED nanoscopy by time gating. *Nat. Methods* 8, 571–573
- 71 Willig, K.I. *et al.* (2006) Nanoscale resolution in GFP-based microscopy. *Nat. Methods* 3, 721–723
- 72 Drobizhev, M. *et al.* (2011) Two-photon absorption properties of fluorescent proteins. *Nat. Methods* 8, 393–399
- 73 Chen, X. *et al.* (2011) Functional mapping of single spines in cortical neurons *in vivo*. *Nature* 475, 501–505
- 74 Svoboda, K. and Yasuda, R. (2006) Principles of two-photon excitation microscopy and its applications to neuroscience. *Neuron* 50, 823–839
- 75 Egeblad, M. *et al.* (2008) Visualizing stromal cell dynamics in different tumor microenvironments by spinning disk confocal microscopy. *Dis. Model. Mech.* 1, 155–167
- 76 Maddox, P.S. (2008) Confocal imaging of cell division. *Curr. Protoc. Cytom.* Chapter 12, Unit 12.11
- 77 Summers, J.A. *et al.* (2010) High contrast, depth-resolved thermoreflectance imaging using a Nipkow disk confocal microscope. *Rev. Sci. Instrum.* 81, 014902
- 78 Dani, A. *et al.* (2010) Superresolution imaging of chemical synapses in the brain. *Neuron* 68, 843–856
- 79 Frost, N.A. *et al.* (2010) Single-molecule discrimination of discrete perisynaptic and distributed sites of actin filament assembly within dendritic spines. *Neuron* 67, 86–99
- 80 Vaziri, A. and Shank, C.V. (2010) Ultrafast widefield optical sectioning microscopy by multifocal temporal focusing. *Opt. Express* 18, 19645–19655